THE JOURNAL OF PHYSICAL CHEMISTRY B
A JOURNAL OF THE AMERICAN CHEMICAL SOCIETY

pubs.acs.org/JPCB

Article

Impact of Anticancer Polymers on Model Cancerous Membranes: Molecular-Level Insight from Computer Simulations

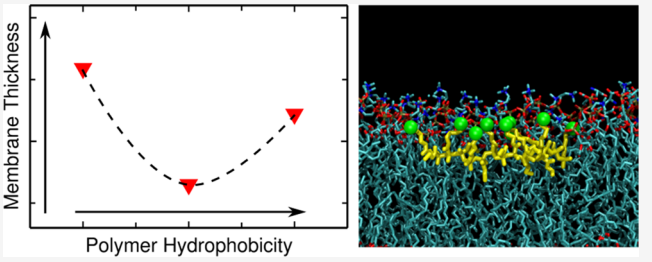
Andrey A. Gurtovenko* and Victor M. Nazarychev

Cite This: *J. Phys. Chem. B* 2026, 130, 9816–9825

Read Online

ACCESS | Metrics & More | Article Recommendations | Supporting Information

ABSTRACT: Anticancer polymers represent a novel, promising class of therapeutical agents aimed to combat emerging multidrug resistance. Here, we employ atomic-scale computer simulations to explore for the first time the molecular-level impact of anticancer polymers on model cancerous membranes. To this end, we focused on methacrylate-based random copolymers with proven anticancer activity. Our computational findings show that phosphatidylserine lipids on the surface of cancerous membranes serve as the primary targets for protonated amine groups of anticancer polymers. Adsorption of cationic anticancer polymers induces the lateral ordering and clustering of anionic phosphatidylserines in line with existing experimental data. Embedding polymers into the membrane results in an expansion of the membrane, which is accompanied by a drop in its thickness and by disordering of lipid acyl chains. Within the membrane, anticancer polymers adopt a comb-like conformation with the backbones being buried in the hydrophobic membrane core and the protonated side groups being bound to lipid phosphate groups. The polymer-induced thinning of the membrane turns out to depend non-monotonically on polymer hydrophobicity. This highlights the importance of a balance between the overall charge and the hydrophobicity of polymers for promoting anticancer activity. Although spontaneous pore formation was shown to be beyond the time scales accessible through atomic-scale simulations, membrane thinning can be considered a first step toward the nucleation of transmembrane pores and subsequent membrane collapse. Our electroporation tests showed that the membrane became more prone to poration upon adsorption of anticancer polymers. All in all, our computational findings provide valuable microscopic information for further optimization of anticancer polymeric agents.



INTRODUCTION

One of the major challenges in cancer therapy is related to emerging multidrug resistance. Cancer evolution has led to a situation when cancer cells became resistant to structurally distinct drugs with various mechanisms of action.[1] As a result, there is a substantial demand for novel anticancer agents that could overcome the existing drug resistance. In this regard, anticancer polymers represent a promising class of therapeutic alternatives for combating tumors.[2] Such polymers have many advantages, including lower *in vivo* degradation compared to anticancer peptides, scalable mass production, and low cost.[3] Anticancer polymers are often inspired by antimicrobial polymers: they represent cationic species that specifically target the surface of cancer cells.[4] Similar to bacteria, cancer cells have a negatively charged surface[5] due to several factors, with the main one being the overexpression of negatively charged phosphatidylserine (PS) lipids on the outer leaflet of cancerous cell membranes.[6]

As far as important representatives of anticancer polymers are concerned, Kuroda et al. recently reported methacrylate-based random copolymers that exhibited cytotoxicity to prostate cancer cells.[7] The anticancer polymers were built from cationic and hydrophobic monomeric units; the charged monomers contained primary amine groups that mimicked lysine residues of anticancer peptides. The authors showed that anticancer activity could be tuned through adjusting monomer composition: the optimal impact on cancer cells was achieved when the ratio of cationic-hydrophobic groups was set to 2:1 (the polymer P-5 in ref 7). A further increase in hydrophobicity had no noticeable effect on anticancer activity but led to a more severe lysis of non-cancerous normal cells. Furthermore, in addition to cancer cells, the authors demonstrated that the polymer P-5 promoted the lysis of giant unilamellar vesicles consisting of the mixture of zwitterionic and anionic lipids. In our study we employed atomic-scale molecular dynamics simulations to get a detailed insight into the impact of the anticancer methacrylate-based polymers on model cancerous membranes.

To the best of our knowledge, there have been no published computational studies on anticancer polymers. However, the

Received: May 31, 2026
Revised: August 24, 2026
Accepted: September 8, 2026
Published: September 12, 2026



ACS Publications © 2026 American Chemical Society

https://doi.org/10.1021/acs.jpcb.6c03563
J. Phys. Chem. B 2026, 130, 9816–9825

Downloaded from pubs.acs.org/jpcbfk/article-pdf/130/38/9816/6849226O/acs.jpcb.6c03563.pdf?guestAccessKey=68260e30-8a50-43a7-b021-503799ebd130 by Andrey Gurtovenko on 24 September 2026

above-mentioned methacrylate-based random copolymers have been considered via computer simulations in the context of their antimicrobial activity.[8] In particular, it was shown that methacrylate-based copolymer chains built from protonated and hydrophobic monomers electrostatically attracted to model bacterial membranes; the latter was represented as a mixture of zwitterionic phosphatidylethanolamine and anionic phosphatidylglycerol lipids. The protonated amine groups of the polymers interacted with the phosphate region of lipid head groups, while hydrophobic monomers were embedded into the membrane interior.[9] Further studies have explored the effect of the lipid composition of model membranes on polymer−lipid interactions.[10] Recently, a third type of monomer (a polar residue[11,12] or an anionic residue[13]) was added to cationic and hydrophobic monomeric units, and the impact of the ternary methacrylate copolymers on model bacterial membranes was systematically studied.

In our study, we probe for the first time the molecular details of the interaction between anticancer methacrylate-based copolymers and model cancerous membranes. Here we closely follow the experimental study by Kuroda et al.[7] and consider binary copolymers of the same chemical structure and the same molecular weight as in ref 7. We systematically varied the content of hydrophobic monomers in a polymer chain and explored how the ratio of protonated and hydrophobic monomeric units affects the impact of the polymers on model cancerous membranes.

MATERIALS AND METHODS

We have performed atomic-scale molecular dynamics simulations to explore the interactions between anticancer methacrylate-based polymers and model cancerous membranes. In our study, we focused on random methacrylate-based copolymers with proven anticancer activity as reported in a recent experimental work.[7] Overall, we considered three anticancer polymers, see Table 1 and Figure 1. P5 and P6 polymers closely reproduce the chemical structure and the degree of polymerization of synthesized random copolymers P-5 and P-6, which showed the highest anticancer activity.[7] In simulations, the protonated and hydrophobic monomers were evenly distributed over the polymer chain; the end groups present in the synthesized polymers P-5 and P-6 were truncated to simplify the chemical structure.[7−9] The ratio of charged/hydrophobic monomers was 2:1 (P5) and 1:1 (P6). For completeness, we also considered the polymer P7, which has a mirrored chemical structure with respect to P5, see Table 1 and Figure 1. P7 is the most hydrophobic polymer in a series (the ratio of charged/hydrophobic units is 1:2), and its anticancer activity was not assessed experimentally.[7]

Table 1. Anticancer Methacrylate-Based Random Copolymers[a]

polymers	$N_{monomer}$	$N_{charged}$	$N_{neutral}$	ratio
P5	16	11	5	2:1
P6	17	9	8	1:1
P7	16	5	11	1:2

[a]Shown are the degree of polymerization, $N_{monomer}$, the numbers of charged and neutral monomers, $N_{charged}$ and $N_{neutral}$, and the ratio of charged and hydrophobic monomeric units.

A membrane of cancer cells was modelled as a mixture of zwitterionic dioleoyl-phosphatidylcholine (DOPC) and anionic dioleoyl-phosphatidylserine (DOPS) lipids. It is generally accepted that externalization of PS lipids is a common feature of cancerous cells.[6,14] Our choice of lipids was dictated by ref 7 in which the authors studied the impact of anticancer polymers on giant unilamellar DOPC/DOPS vesicles. They considered 2 concentrations of PS lipids (10 and 35 mol %) and showed that the polymer-induced lysis of the vesicles was only slightly affected by the PS content in the lipid membrane.[7] In our study, we chose to study a relatively high concentration of PS lipids (35 mol %) in a model cancerous membrane to speed up the binding of cationic polymer chains to the anionic membrane surface. Our model membrane system consisted of 256 lipids (166 DOPC and 90 DOPS lipids).

The full-atom CHARMM General Force Field (CGenFF, version 4.6)[15] was used for polymers, while lipids were described by the CHARMM36 force field.[16] Water molecules were represented by the CHARMM version of the TIP3P model.[17] Molecular dynamics (MD) simulations were performed with the use of the v-rescale thermostat[18] and the C-rescale barostat.[19] Pressure was set to 1 bar and controlled isotropically in simulations of polymer solutions; for polymer-membrane systems, the semi-isotropic pressure coupling was used. Constraints were applied to all bonds with hydrogen atoms. The Lennard-Jones interactions were cut off at 1.2 nm; the forces were smoothly switched to zero between 1.0 and 1.2 nm. Electrostatic interactions were handled using the particle-mesh Ewald (PME) method.[20] The time step of 2 fs was used; periodic boundary conditions were applied in all directions. For all simulations, the Gromacs 2023 simulation suite[21] was used.

The CGenFF server[22] was used to generate the initial structures and force field parameters for monomers of anticancer methacrylate-based copolymers. The monomers were connected into a polymer chain using the Gromacs simulation suite (the *gmx pdb2gmx* tool).[21] Before actual polymer-membrane simulations, polymers in aqueous solution were studied. Eight copies of each polymer (P5, P6, and P7) were solvated in a cubic box. The systems were neutralized by chloride ions; 0.15 M of KCl salt was additionally placed in the water phase. Each polymer solution was simulated for 1 μs at the physiological temperature of 310 K, see Table 2. The initial structure of a DOPC/POPS lipid membrane was generated using the CHARMM-GUI Membrane Builder.[23] After solvation, neutralization by potassium ions, and adding salt (0.15 M of KCl), the membrane was simulated for 1 μs at various temperatures, see Table 2. This membrane system will be used as a reference for assessing the impact of anticancer polymers on model lipid membranes.

Due to the inherent limitations of atomic-scale MD simulations in terms of the time scales accessible, we set up the polymer-membrane systems with a special emphasis on enhanced sampling. First, we consider a relatively high concentration of polymers. Second, we focus on the binding of polymers to both leaflets of the membrane, although in experiments anticancer polymers interacted with the outer membrane leaflet only.[7] Preventing one of the monolayers from being in contact with polymers could hinder the defect formation in membranes and require longer simulation times. An additional advantage of the symmetrical polymer binding is in the independent adsorption of polymers on both membrane leaflets, which enhances the sampling. And third, as polymer embedding into the membrane interior is a slow process,[24,25]

Downloaded from pubs.acs.org/jpcbfk/article-pdf/130/38/9816/6849260/acs.jpcb.6c03563.pdf?guestAccessKey=68260e30-8a50-43a7-b021-503799ebd130 by Andrey Gurtovenko on 24 September 2026

https://doi.org/10.1021/acs.jpcb.6c03563
J. Phys. Chem. B 2026, 130, 9816−9825

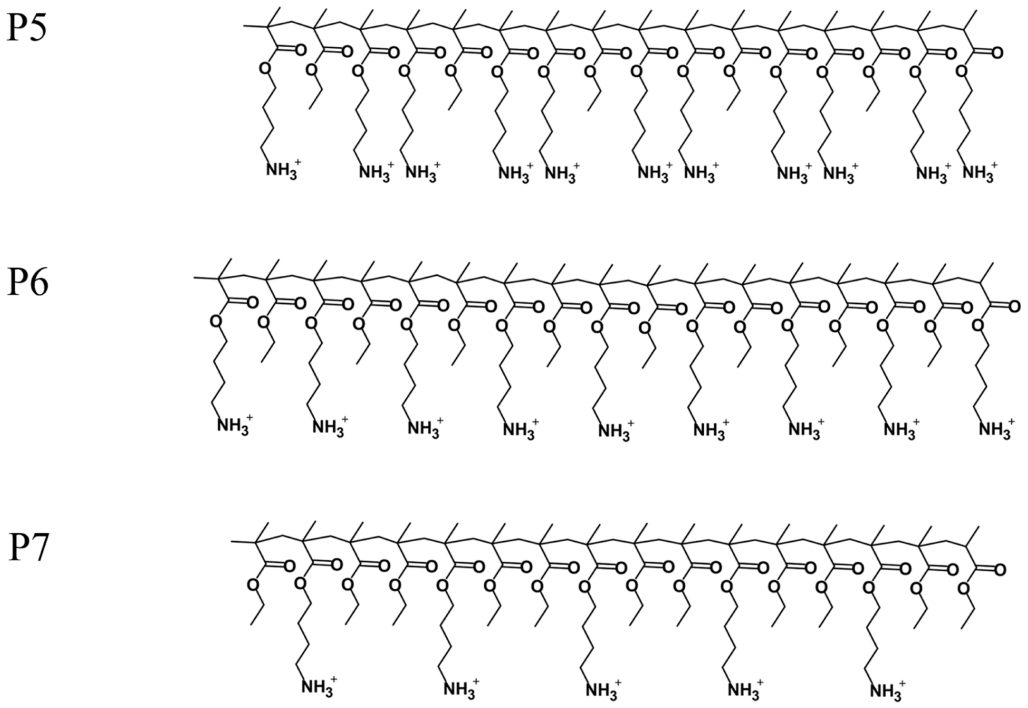


Figure 1. Chemical structure of anticancer methacrylate-based copolymers P5, P6, and P7.

Table 2. Simulated Systems[a]

	polymers	DOPC	DOPS	water	atoms	time
P5	8	–	–	41,888	129,104	1 μs (T = 310 K)
P6	8	–	–	41,958	129,298	1 μs (T = 310 K)
P7	8	–	–	42,117	129,311	1 μs (T = 310 K)
PCPS	–	166	90	13,991	76,907	1 μs (T = 310 K)
						1 μs (T = 363 K)
						1 μs (T = 423 K)
PCPS-Electro	–	166	90	13,991	76,907	20 × (0.1−0.25 μs)
						(T = 363 K)
PCPS-P5	16	166	90	26,161	119,715	6 μs (T = 310 K)
						6 μs (T = 363 K)
						5 μs (T = 423 K)
PCPS-P6	16	166	90	26,212	119,836	6 μs (T = 310 K)
						5 μs (T = 363 K)
						5 μs (T = 423 K)
PCPS-P7	16	166	90	26,542	119,918	5 μs (T = 310 K)
						5 μs (T = 363 K)
						5 μs (T = 423 K)
PCPS-P6-Electro	16	166	90	26,212	119,836	20 × (0.1−0.25 μs)
						(T = 363 K)

[a]Shown are the number of polymers, DOPC lipids, DOPS lipids, and water molecules; the total number of atoms and the simulation time.

we perform MD simulations at elevated temperatures. This is a standard approach to enhance sampling, and it is routinely used in computer simulations of antimicrobial peptides (AMPs) due to the thermostability of the α-helical structure of most AMPs in the lipid environment.[26−28] Anticancer polymers are structurally simpler than AMPs, as their action is not linked to a certain secondary structure. Therefore, one can expect that high-temperature simulations could be a valuable tool for polymers.

Overall, each polymer-membrane system consisted of a DOPC/DOPS lipid membrane and 16 polymer chains (the polymer-to-lipid ratio was set to 1/16). Initially, polymer chains were distributed symmetrically with respect to the membrane and placed in the water phase in the vicinity of both leaflets. After solvating and adding 0.15 M of KCl salt, a short, 5 ns pre-equilibration run with restrained polymers was carried out. Position restraints were applied to all non-hydrogen atoms of polymers in all three directions. After that, all position restraints were removed, and multi-microsecond simulations were performed at the physiological temperature of 310 K and also at elevated temperatures of 363 and 423 K, see Table 2. For the sake of comparison, a polymer-free membrane system, PCPS, was simulated at three temperatures (310, 363, and 423 K), see Table 2. Note that in this study, the elevated

https://doi.org/10.1021/acs.jpcb.6c03563
J. Phys. Chem. B 2026, 130, 9816−9825

Downloaded from pubs.acs.org/jpcbfk/article-pdf/130/38/9816/6849226O/acs.jpcb.6c03563.pdf?guestAccessKey=68260e30-8a50-43a7-b021-503799ebd130 by Andrey Gurtovenko on 24 September 2026

temperatures of 363 and 423 K have no physiological relevance and are used to enhance the sampling.

To explore whether the model cancerous membrane becomes more prone to poration upon adsorption of anticancer polymers, we performed a series of simulations with an applied external electric field. For two systems (PCPS-Electro and PCPS-P6-Electro), we varied the strength of the electric field to evaluate the pore formation time at T = 363 K. All in all, the external electric field was set to 0.225, 0.25, 0.3, and 0.4 V/nm for the PCPS-Electro system and to 0.1, 0.15, 0.2, and 0.3 V/nm for the PCPS-P6-Electro system. The simulations were repeated 5 times with different initial conditions for each magnitude of the electric field. The simulation runs were 100−250 ns long, depending on the applied field, see Table 2.

RESULTS AND DISCUSSION

Prior to polymer-membrane systems, we performed microsecond-long simulations of polymer solutions (8 polymer chains in aqueous solution with 0.15 M of KCl salt). As all three types of polymers have hydrophobic monomeric units (Figure 1), these simulations were aimed at shedding light on possible aggregation behavior of the polymers. To quantify the polymer aggregation, we carried out a cluster analysis of polymer chains in solution with the use of the Gromacs tool *gmx clustsize*.[21] It turns out that polymers P5 and P6 do not aggregate, while polymers P7 form small clusters containing on average 2.0 ± 0.4 chains. Such behavior of P7 polymers is not surprising, as P7 is the most hydrophobic polymer in the series, see Figure 1 and Table 1. As we proceed to show, the aggregation of P7 polymers will affect the interactions of the polymers with model cancerous membranes.

To explore the impact of anticancer polymers on model lipid membranes, 16 polymer chains were placed in water symmetrically with respect to the membrane, and multi-microsecond MD simulations were performed at various temperatures. To speed up the polymer adsorption, we focused on a relatively high concentration of polymers (polymer-to-lipid ratio was set to 1/16). The initial binding of cationic polymers to the anionic surface of a membrane was driven by the electrostatic attraction. However, to achieve stable binding to the membrane, a polymer chain should embed deeper into the membrane interior, which requires much longer times. Embedding polymer chains results in the membrane expansion. Therefore, to monitor equilibration, we followed the time evolution of the area per lipid. Note that lipid bilayers are almost incompressible in terms of volume; as a result, the equilibration of the area per lipid implies that other important quantities, such as the membrane thickness and the volume per lipid, are also equilibrated. Nevertheless, in addition to the area per lipid, we also followed the time evolution of the membrane thickness to ensure that equilibration is achieved. It turns out that at low temperatures (T = 310 K), the equilibration of polymer-membrane systems takes several microseconds. At higher temperatures (363 and 423 K), the equilibration occurs faster; nevertheless, high-temperature simulations were also extended to 5−6 μs, see Table 2.

In Figure 2A we present the average values of the area per lipid for all simulated membrane systems at various temperatures. If not stated otherwise, all structural characteristics are averaged over the last microsecond of the trajectory for polymer-membrane systems and over the last 500 nanoseconds

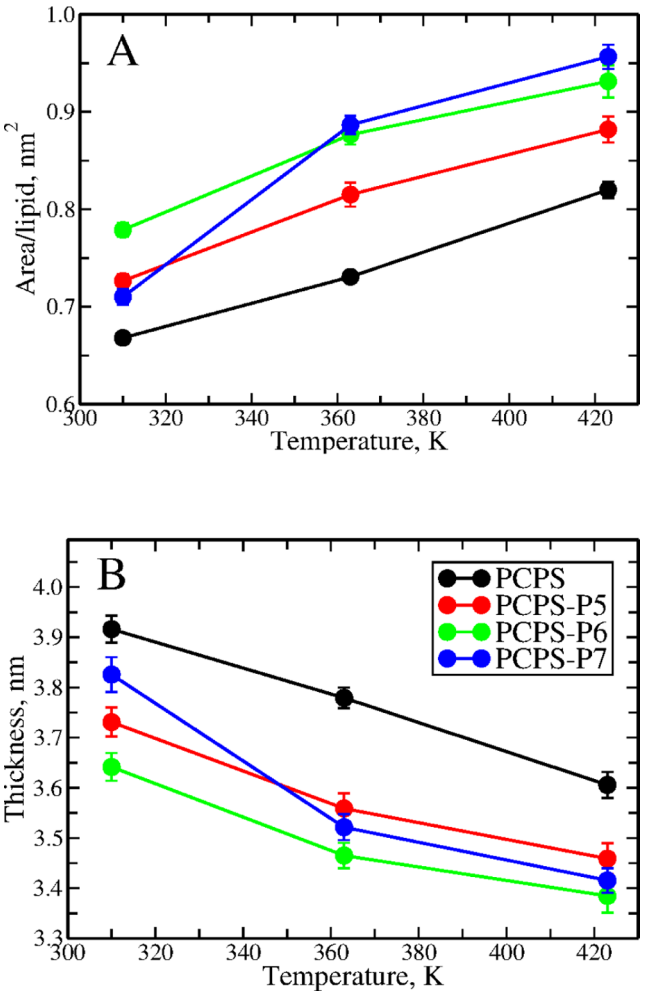


Figure 2. (A) The area per lipid at various temperatures. (B) The thickness of the membrane at various temperatures. Shown are results for a polymer-free DOPC/DOPS membrane as well as for the membrane interacting with P5, P6, and P7 polymers.

for the polymer-free membrane system; the errors are standard deviations calculated over 10 ns blocks.

As seen, increasing the temperature leads to a systematic increase in the area per lipid for a polymer-free membrane system. For polymer-membrane systems, we observe an additional growth of the area per lipid due to embedding polymers into the membrane (Figure 2A). The impact of P5 and P6 polymers can be directly linked to the hydrophobicity of the polymers: more hydrophobic polymers, P6, embed deeper into the membrane, leading to a larger area per lipid. This relative difference in the impact of P5 and P6 is also observed at elevated temperatures (363 and 423 K). However, the corresponding absolute values of the area per lipid show a noticeable increase with temperature, implying that heating the systems promotes more polymers to partition into the membrane, see Figure 3.

As far as the polymers P7 are concerned, the situation is more involved. At the physiological temperature (310 K), the area per lipid for the PCPS-P7 system is lower than that of P5 and P6 counterparts (Figure 2A), although P7 polymers are more hydrophobic. This is due to the above-mentioned aggregation of P7 polymers in the water phase; some of these aggregates are seen in Figure 3 even after 5 μs simulations. To adsorb on the membrane surface, polymer chains should first

Downloaded from pubs.acs.org/jpcbfk/article-pdf/130/38/9816/6849226O/acs.jpcb.6c03563.pdf?guestAccessKey=68260e30-8a50-43a7-b021-503799ebd130 by Andrey Gurtovenko on 24 September 2026

https://doi.org/10.1021/acs.jpcb.6c03563
J. Phys. Chem. B 2026, 130, 9816−9825

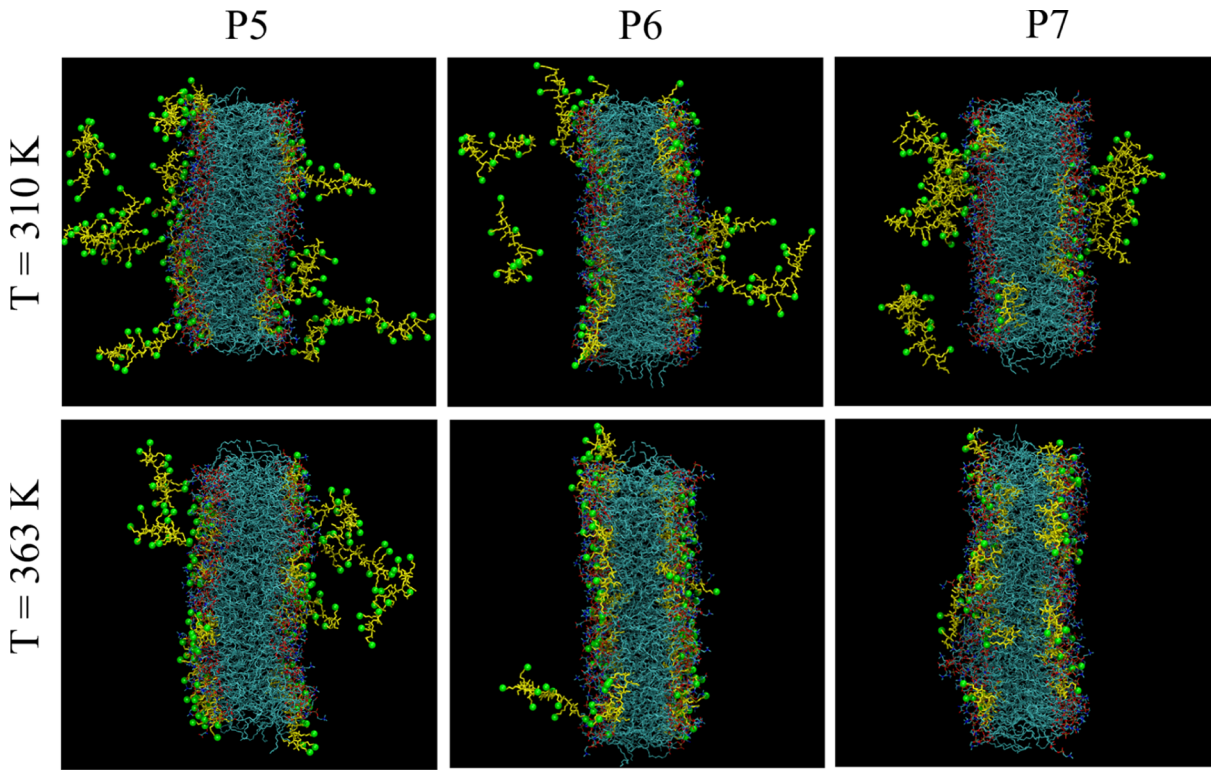


Figure 3. Snapshots of three polymer-membrane systems at two temperatures (310 and 363 K). Shown are the final configurations at the end of multi-microsecond simulation runs (5−6 μs). Lipid membranes are shown in cyan, polymers are shown in yellow, and protonated amine groups are presented as green spheres; water and ions are not shown. The snapshots were prepared using the VMD visualization software.[29]

leave the aggregates, which is a slow process at a relatively low temperature of 310 K. Therefore, the aggregation of P7 polymers slows down the kinetics of polymer adsorption on the membrane surface. However, this aggregation does not affect the final binding of P7 polymers. Indeed, heating the system to 363 K destroys these aggregates and allows P7 chains to embed into the membrane. Importantly, the area per lipid practically coincides for PCPS-P6 and PCPS-P7 systems at T = 363 K and T = 423 K, most likely due to the partition of all polymer chains in the membrane, see Figures 2A and 3.

Similar conclusions can also be drawn from the membrane thickness presented in Figure 2B, as the increase in the area per lipid normally leads to a drop in thickness. The only noticeable difference is in the non-monotonic dependence of the membrane thickness on polymer hydrophobicity at elevated temperatures of 363 and 423 K. In spite of the fact that the area per lipid for PCPS-P7 is a bit larger than that for PCPS-P6, P7 polymers lead to a smaller membrane thinning compared to P6 (Figure 2). The membrane thickness is measured as the distance between averaged positions of phosphate atoms on the opposite leaflets of the membrane. In addition to the thinning due to the membrane expansion, the partition of polymers in the membrane pulls the phosphate groups towards the membrane interior. However, the number of protonated amine groups that interact with lipids' phosphates is considerably smaller in the case of P7 as compared to P6 (see Table 1), resulting in the observed non-monotonic behavior. Therefore, a subtle balance between the overall charge and hydrophobicity of polymers is essential to promote the membrane thinning, which is often considered a prerequisite for nucleation of pores in lipid membranes.[30−32]

Although we did not observe the formation of transmembrane pores in the considered systems, simulations at elevated temperatures allow us to obtain a rough estimate of the lower boundary for the time scales required for pore formation. To do that, one needs to relate the time scales at the lowest (310 K) and the highest (423 K) temperatures. If the formation of a pore is a thermally activated process, the rate constant of pore formation is determined by $\exp(-\Delta G_{pore}/k_B T)$, where ΔG_{pore} is the free energy of pore formation.[33] Assuming that the free energy ΔG_{pore} does not depend on temperature and taking 80 kJ/mol as a typical value[33] for ΔG_{pore}, we can conclude that the high-temperature simulations (T = 423 K) speed up the process of pore formation by ∼4000 times compared to T = 310 K. Given that we performed simulations on a multi-microsecond time scale, the pore formation in the considered systems requires at least tens of milliseconds at physiological temperature (310 K), which is hardly accessible at present in atomic-scale computer simulations.

Interactions of anticancer polymers with model cancerous membranes are of tremendous importance in terms of targeting these polymeric agents to cancer cells. Experimental studies of the anticancer polymers hypothesized that PS lipids can play a major role for such targeting. In particular, it was shown that anticancer methacrylate-based copolymers P5 led to the lysis of giant unilamellar DOPC/DOPS vesicles but had no impact on their DOPC counterparts.[7] In simulations, we found that protonated amine residues of methacrylate-based copolymers interact considerably stronger with phosphate groups of DOPS lipids compared to those of DOPC lipids, as seen from the corresponding radial distribution functions (RDFs), see Figure 4. This selectivity of anticancer polymers to

https://doi.org/10.1021/acs.jpcb.6c03563
J. Phys. Chem. B 2026, 130, 9816−9825

Downloaded from pubs.acs.org/jpcbfk/article-pdf/130/38/9816/6849260/acs.jpcb.6c03563.pdf?guestAccessKey=68260e30-8a50-43a7-b021-503799ebd130 by Andrey Gurtovenko on 24 September 2026

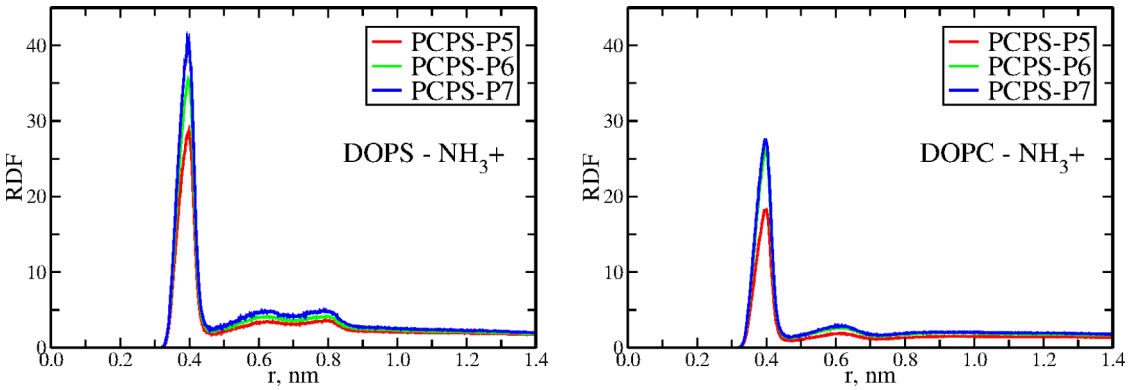


Figure 4. Radial distribution functions (RDFs) of nitrogen atoms of protonated amine groups of anticancer polymers and phosphorus atoms of head groups of anionic DOPS (left) and zwitterionic DOPC (right) lipids at T = 363 K.

PS lipid head groups on the membrane surface resembles the similar preferential binding of antimicrobial cationic polymers to anionic phosphatidylglycerol lipids of model bacterial membranes.[24,25]

A detailed analysis of the number of contacts between protonated polymer groups, NH_3, and lipid phosphate groups, P_{lipid}, again shows a nonmonotonic dependence on polymer hydrophobicity, see Figure 5A. Due to higher hydrophobicity, P6 polymers embed easier into the membrane as compared to P5 (Figure 3) and form more contacts with lipid phosphates, even though a P6 polymer has somewhat smaller number of NH_3 groups, see Table 1 (9 for P6 versus 11 for P5). As a result, the number of NH_3−P_{lipid} contacts for P6 is larger than for P5, see Figure 5A. In contrast, the most hydrophobic polymer P7 has only 5 protonated amine groups, which is ∼2 times smaller than for P5 and P6. Therefore, the number of NH_3−P_{lipid} contacts is also noticeably smaller, despite the higher hydrophobicity, as seen in Figure 5A. On the other hand, the small number of charged groups along with deeper partition of P7 polymers into the membrane interior results in a superiority of P7 over the rest of the polymers in terms of the fraction of NH_3 groups that are in contact with lipid phosphates at elevated temperatures (Figure 5B).

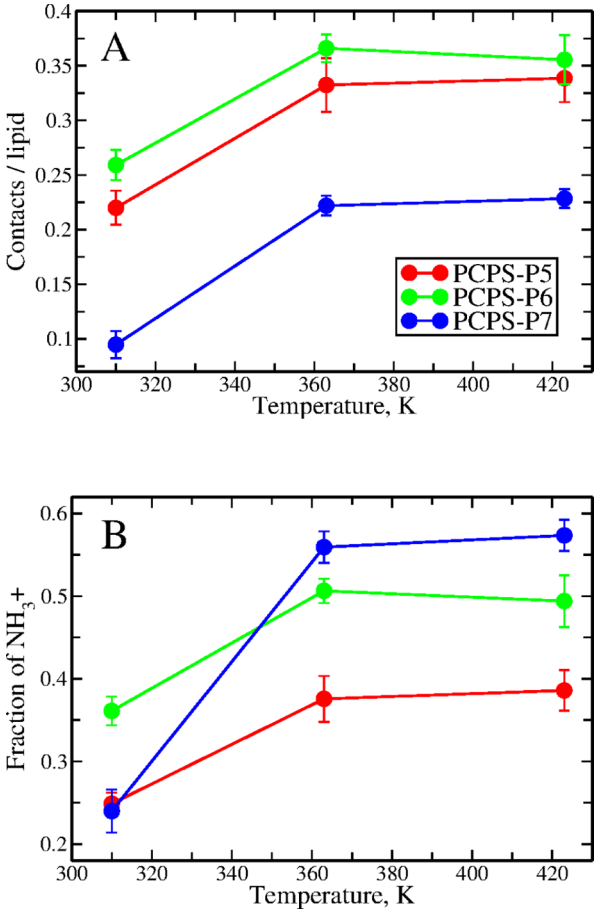


Figure 5. (A) The number of contacts (per lipid) of protonated polymer groups, NH_3, with lipid phosphate groups, P_{lipid}, at different temperatures. (B) The fraction of protonated amine groups that are in contact with lipid phosphates at different temperatures.

Another important conclusion to be drawn from Figure 5 is related to the convergence of high-temperature simulations. Heating the polymer-membrane systems from 310 to 363 K speeds up considerably the partition of anticancer polymers in the membrane. In turn, simulations at an even higher temperature of 423 K do not lead to any noticeable changes in the number of NH_3−P_{lipid} contacts and in the fraction of protonated amine groups that are in contacts with lipid phosphates, see Figure 5. This implies that the MD simulations at T = 363 K are most likely converged. This is especially important because such high temperatures can be employed in experiments, for instance, to probe the thermostability of anticancer peptides such as cecropin.[34,35] Therefore, for the rest of the paper we will limit the discussion to the high-temperature simulations at T = 363 K.

While anionic PS lipids are essential for initial binding of cationic anticancer polymers to the surface of a model cancerous membrane, the adsorbed polymers can also affect the lateral distribution of lipids. To explore this, we calculated two-dimensional radial distribution functions (2D RDFs) for PS lipids, see Figure 6. First off, a 2D RDF of PS lipids in a polymer-free DOPC/DOPS membrane has a pronounced first peak, which corresponds to a certain lateral clustering of anionic lipids even without polymers. This clustering could be lipid- and force field-specific. For instance, 2D RDFs for anionic phosphatidylglycerol lipids in a phosphatidylethanolamine/phosphatidylglycerol membrane described by the AMBER force field did not develop any peaks.[24] In turn, adding anticancer polymers to the membrane system makes the peak of 2D RDFs of PS lipids noticeably higher, see Figure 6. This implies that anionic DOPS lipids become more ordered on the membrane surface upon adsorption of cationic

https://doi.org/10.1021/acs.jpcb.6c03563
J. Phys. Chem. B 2026, 130, 9816−9825

Downloaded from pubs.acs.org/jpcbfk/article-pdf/130/38/9816/6849226O/acs.jpcb.6c03563.pdf?guestAccessKey=68260e30-8a50-43a7-b021-503799ebd130 by Andrey Gurtovenko on 24 September 2026

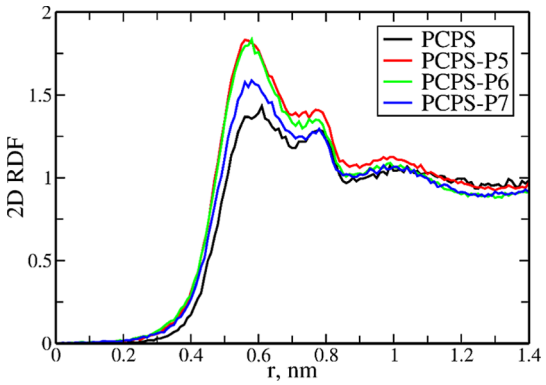


Figure 6. Two-dimensional radial distribution functions of phosphate groups of DOPS lipids at T = 363 K.

anticancer polymers. This is in line with the strong interactions of protonated polymer groups and DOPS lipid phosphate groups as discussed earlier (Figure 4). This effect is weaker for P7 polymers, most likely due to a considerably smaller number of charged amine groups of P7, see Table 1.

We also performed a cluster analysis of DOPS phosphate groups on the membrane surface; the position of the 2D RDF first minimum (0.7 nm) in Figure 6 was used as a cut-off length for two groups to be neighbors. The average number of PS lipids per cluster amounted to 1.44 ± 0.06 for P5, 1.39 ± 0.05 for P6, and 1.32 ± 0.04 for P7. Given that in a polymer-free lipid bilayer, the clusters contain 1.35 ± 0.03 PS lipids, P5 and P6 polymers induce additional lateral clustering of anionic lipids.

Importantly, the observed polymer-induced ordering and clustering of PS lipids is in line with existing experimental data. As shown in ref 36, the binding of cationic polymer polylysine to PC/PS membranes led to the formation of domains enriched in PS lipids on the membrane surface. It is also noteworthy that similar polymer-induced segregation of anionic lipids has also been observed in experimental[37] and computational[24] studies of model bacterial membranes interacting with cationic polylysine chains.

To evaluate the structural changes in DOPC/DOPS lipid membranes upon adsorption of cationic anticancer polymers, we calculated mass density profiles of principal components of polymer-membrane systems, see Figure 7. For a polymer-free system PCPS, we observe lipid and water distributions typical for lipid bilayers. The lipid mass density profile has a well-structural shape with two maxima corresponding to lipid head groups and a minimum in the central membrane region occupied by lipid acyl chains. Water molecules permeate relatively deep into the lipid head group region, forming the lipid/water interface. Embedding anticancer polymers into the membrane has a noticeable impact on the lipid density profile. Accommodation of P5 polymers within the membrane straightens the peaks and the well of the density profile of lipids, while polymers P6 and P7 make the lipid profile flat, see Figure 7. An obvious lack of structure in the lipid density profile implies the disordering effect of anticancer polymers on lipid molecules. It is noteworthy that the polymers partition

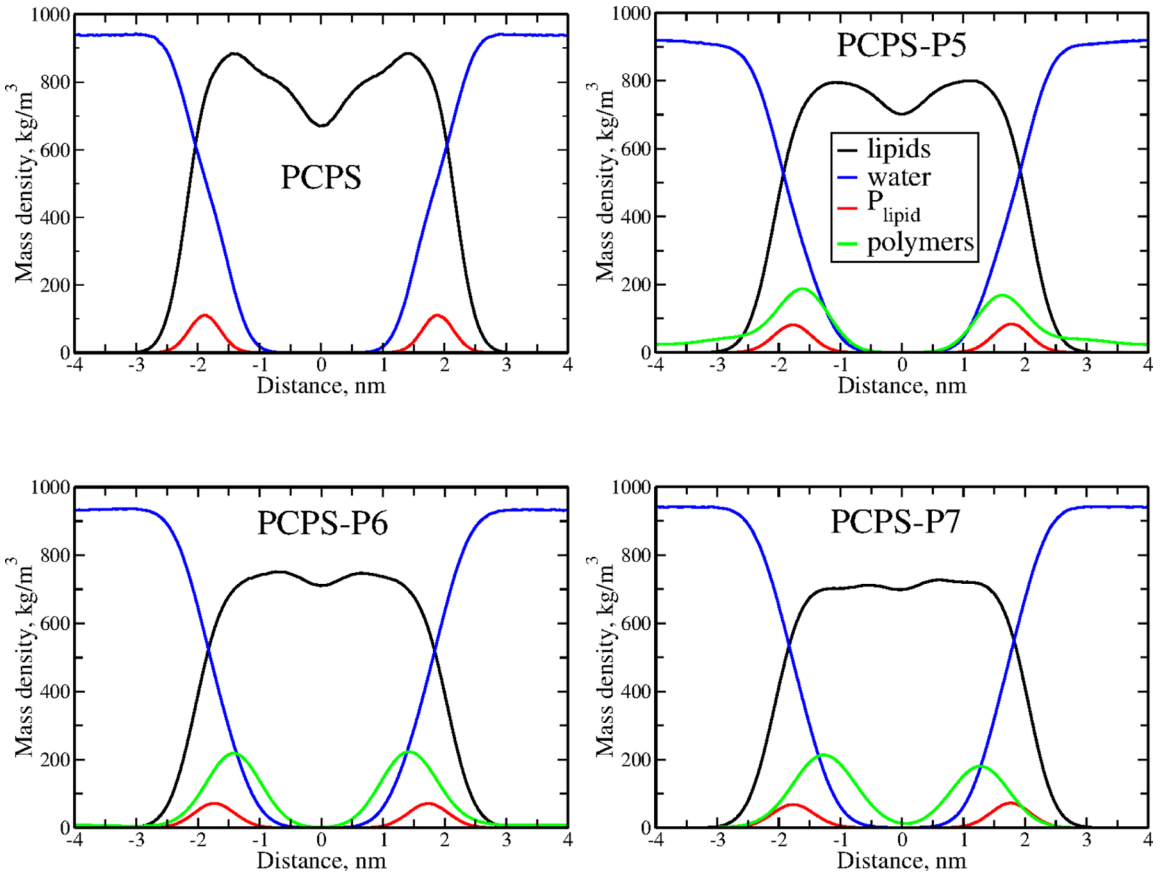


Figure 7. Component-wise mass density profiles for DOPC/DOPS lipid membranes interacting with anticancer polymers. Shown are profiles for lipids, water molecules, and polymers; the profile for lipid phosphate groups is also presented.

https://doi.org/10.1021/acs.jpcb.6c03563
J. Phys. Chem. B 2026, 130, 9816−9825

Downloaded from pubs.acs.org/jpcbfk/article-pdf/130/38/9816/6849226O/acs.jpcb.6c03563.pdf?guestAccessKey=68260e30-8a50-43a7-b021-503799ebd130 by Andrey Gurtovenko on 24 September 2026

deep into the membrane interior, and the relative depth of the polymer insertion has a clear correlation with the hydrophobicity of polymers.

The arrangement of polymer chains within the membrane interior can be clarified through mass density profiles for principal atoms of the polymers, which are presented in Figure 8. It is seen that protonated amine groups of all three types of

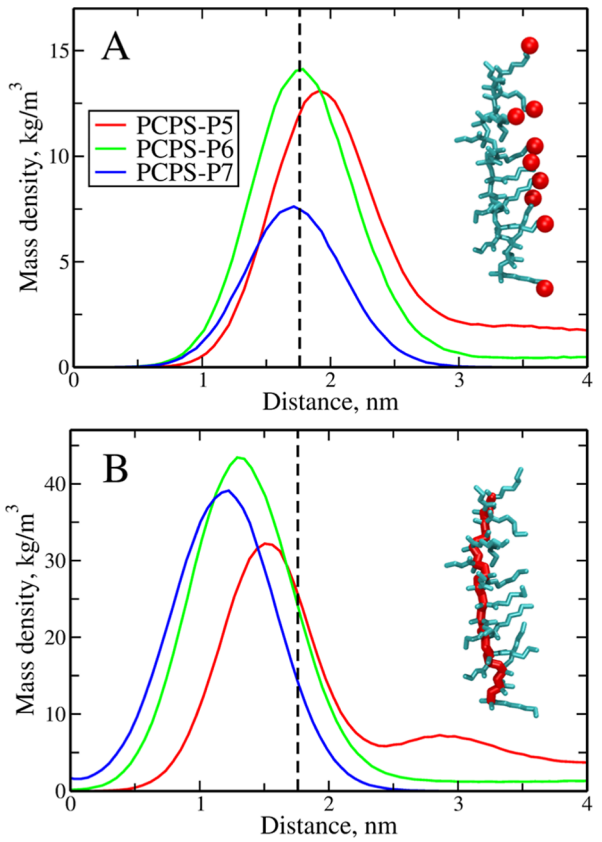


Figure 8. Component-wise mass density profiles for principal atoms of anticancer polymers within a DOPC/DOPS lipid membrane. Shown are results for (A) protonated amine groups of polymers and (B) the polymer backbone. The dashed vertical line corresponds to the approximate location of lipid phosphate groups.

anticancer polymers are localized within the phosphate region of lipids, which is in line with the above-mentioned strong NH_3–P_{lipid} interactions (Figure 8A). In turn, the polymer backbones partition considerably deeper into the membrane interior (beyond the lipid phosphate groups), see Figure 8B. The depth of the partition again correlates well with the polymer hydrophobicity. Taken together, one can conclude that anticancer polymers adopt a comb-like conformation within the DOPC/DOPS membrane: the backbones are buried in the hydrophobic core of the membrane, while protonated side groups are attached to the phosphate region of the membrane, see Figure 8.

The polymer-induced perturbation of the membrane structure, which is seen in Figure 7, can also be characterized through the changes in the ordering of lipid chains. In Figure 9 we present deuterium order parameters of acyl chains of DOPC and DOPS lipids. For a polymer-free system PCPS, deuterium order parameters have a typical shape of lipids with unsaturated hydrocarbon tails. Adsorption of cationic anticancer polymers has a systematic disordering effect on acyl

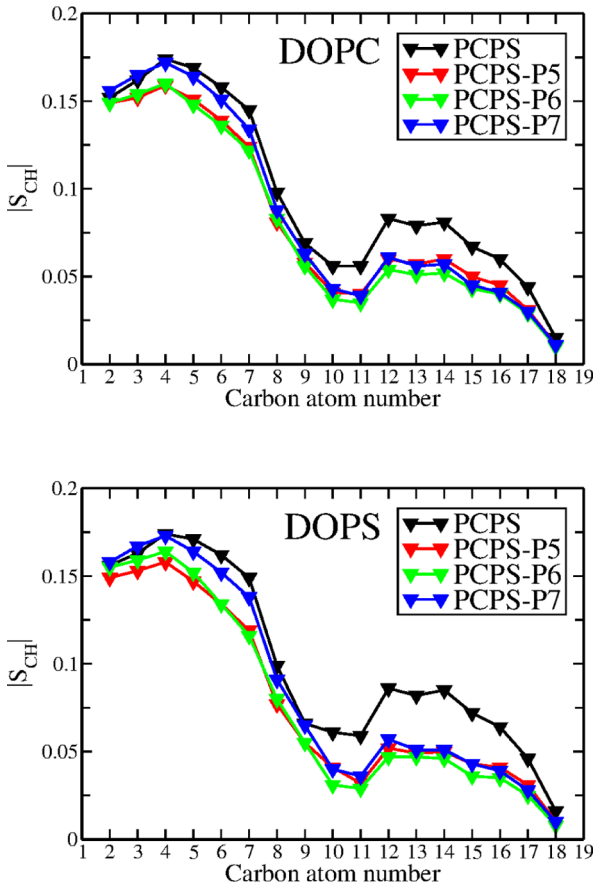


Figure 9. Deuterium order parameters of acyl chains of DOPC (top) and DOPS (bottom) lipids. Small numbers of carbon atoms correspond to those close to lipid head groups.

chains of both DOPC and DOPS lipids. The polymer impact on DOPS lipid chains is somewhat higher than for DOPC counterparts, which is in line with stronger interactions of cationic anticancer polymers with PS phosphate groups (Figure 4). Interestingly, polymers P5 and P6 disorder the entire acyl chains, while the effect of P7 polymers starts only from carbon atom 10 and extends to the end of the acyl chains. It is likely linked to the fact that a P7 polymer has just 5 protonated amine groups (compared to 11 for P5 and 9 for P6) and, therefore, perturbs acyl chains near lipid head groups to a lesser extent compared to P5 and P6 polymers.

The disordering of lipid acyl chains along with membrane thinning discussed earlier can be considered first steps towards the poration of model cancerous membranes by anticancer polymers. As mentioned above, the pore formation process is not accessible through atomic-scale computer simulations for the system at hand. However, we can use an external electric field to demonstrate that the membrane indeed becomes more prone to pore formation upon polymer adsorption. In Figure 10 we present the poration time as a function of the applied electric field[31] for the polymer-free membrane and for the membrane system with P6 polymers. It is seen that the system with P6 polymers requires noticeably weaker electric fields for poration compared to its polymer-free counterpart. Therefore, anticancer polymers do make the model membrane more prone to the formation of transmembrane pores.

https://doi.org/10.1021/acs.jpcb.6c03563
J. Phys. Chem. B 2026, 130, 9816−9825

Downloaded from pubs.acs.org/jpcbfk/article-pdf/130/38/9816/6849260/acs.jpcb.6c03563.pdf?guestAccessKey=68260e30-8a50-43a7-b021-503799ebd130 by Andrey Gurtovenko on 24 September 2026

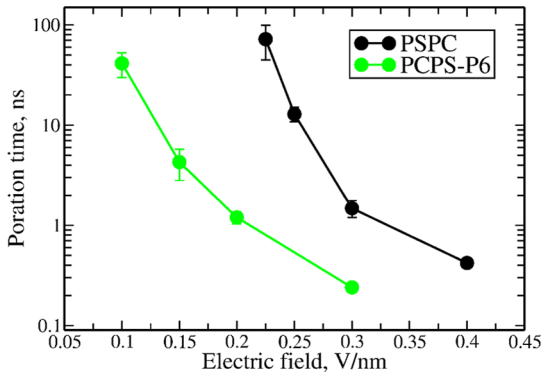


Figure 10. Poration time as a function of the applied electric field at T = 363 K (semilogarithmic coordinates). Shown are results for the polymer-free model membrane (PCPS-Electro) and for the membrane with P6 polymers adsorbed (PCPS−P6-Electro). The errors are standard errors of the mean calculated over five replica simulations.

CONCLUSIONS

In this paper, we report the first computational study of anticancer polymers interacting with model cancerous membranes. These polymers represent a novel, promising class of antitumor therapeutics aimed to overcome emerging multidrug resistance. Here we focused on cationic methacrylate-based random copolymers with proven activity against prostate cancer cells as well as mixed phosphatidylcholine/phosphatidylserine lipid vesicles as a model of cancerous cell membranes.[7] We systematically varied the ratio of protonated and hydrophobic monomers in polymer chains (2:1, 1:1, and 1:2) and employed atomic-scale molecular dynamics simulations to get a detailed insight into the interactions of the anticancer polymers with cellular membranes.

Our computational findings show that cationic anticancer polymers have a tremendous impact on the structural properties of lipid membranes. Anionic phosphatidylserine lipids on the membrane surface are shown to be the primary targets for protonated amine groups of anticancer polymers. This is important in view of the targeting of polymeric agents to cancerous cells that are characterized by the phosphatidylserine externalization. What is more, adsorption of cationic anticancer polymers induces lateral ordering and clustering of anionic phosphatidylserine lipids. This result agrees with experimental data on the formation of domains enriched in phosphatidylserine lipids due to adsorption of cationic polymers.[36]

Embedding polymers into the membrane results in a considerable expansion of the membrane, which is accompanied by a drop in its thickness and by systematic disordering of lipid acyl chains upon polymer adsorption. The depth of polymer partition into the membrane correlates well with polymer hydrophobicity. In the interior of the membrane, anticancer polymers adopt a comb-like conformation with the backbones being buried in the hydrophobic membrane core and the protonated side groups being bound to the region of lipid phosphate groups. Interestingly, the decrease in membrane thickness depends non-monotonically on polymer hydrophobicity: the most hydrophobic polymer considered in our study possesses a relatively small number of protonated amine groups and therefore has a limited ability to pull the lipid phosphate groups towards the membrane interior. This finding highlights the importance of a balance between the overall charge of an anticancer polymer and its hydrophobicity to promote the membrane thinning.

Due to time-scale limitations of atomic-scale computer simulations, we did not witness the polymer-induced formation of transmembrane pores. Our estimates based on high-temperature simulations show that the pore formation requires at least tens of milliseconds at the physiological temperature. However, the observed drop in membrane thickness is an important sign on its own, as such thinning is often considered a prerequisite for nucleation of pores in model cell membranes.[30,32] Indeed, simulations with an external electric field proved that the model membrane became more prone to pore formation upon adsorption of anticancer polymers.

ASSOCIATED CONTENT

Data Availability Statement

Production trajectories and final configurations for all membrane and membrane-polymer systems are available in a repository on Zenodo (10.5281/zenodo.22079842).

Supporting Information

The Supporting Information is available free of charge at https://pubs.acs.org/doi/10.1021/acs.jpcb.6c03563.

Complete description of force field parameters for P5, P6, and P7 polymers in the Gromacs format (PDF)

AUTHOR INFORMATION

Corresponding Author

Andrey A. Gurtovenko − *Branch of Petersburg Nuclear Physics Institute Named By B. P. Konstantinov of National Research Centre "Kurchatov Institute" − Institute of Macromolecular Compounds, Saint Petersburg 199004, Russia; Institute of Chemistry, St. Petersburg State University, 199034 Saint Petersburg, Russia;* orcid.org/0000-0002-9834-1617; Email: a.gurtovenko@gmail.com

Author

Victor M. Nazarychev − *Branch of Petersburg Nuclear Physics Institute Named By B. P. Konstantinov of National Research Centre "Kurchatov Institute" − Institute of Macromolecular Compounds, Saint Petersburg 199004, Russia; Institute of Chemistry, St. Petersburg State University, 199034 Saint Petersburg, Russia;* orcid.org/0000-0003-2448-8584

Complete contact information is available at: https://pubs.acs.org/10.1021/acs.jpcb.6c03563

Notes

The authors declare no competing financial interest.

ACKNOWLEDGMENTS

This work was supported by a grant of the Ministry of Science and Higher Education of the Russian Federation for large scientific projects in priority areas of scientific and technological development (grant number 075-15-2024-553). All the simulations were performed using the computational resources of the Branch of Petersburg Nuclear Physics Institute named by B.P. Konstantinov of National Research Centre "Kurchatov Institute"−Institute of Macromolecular Compounds; the equipment of the shared research facilities of HPC resources at Lomonosov Moscow State University; and resources of the Federal collective usage center "Complex for Simulation and

https://doi.org/10.1021/acs.jpcb.6c03563
J. Phys. Chem. B 2026, 130, 9816−9825

Downloaded from pubs.acs.org/jpcbfk/article-pdf/130/38/9816/6849260/acs.jpcb.6c03563.pdf?guestAccessKey=68260e30-8a50-43a7-b021-503799ebd130 by Andrey Gurtovenko on 24 September 2026

Data Processing for Mega-Science Facilities" at NRC "Kurchatov Institute" (http://ckp.nrcki.ru).

REFERENCES

(1) Ge, M.; Chen, X. Y.; Huang, P.; Fleishman, J. S.; Yang, D. H.; Wu, Z. X.; Ke, Z. F.; Chen, Z. S. Understanding and overcoming multidrug resistance in cancer. *Nat. Rev. Clin. Oncol.* **2025**, *22*, 760−780.

(2) Tan, J.; Tay, J.; Hedrick, J.; Yang, Y. Y. Synthetic macromolecules as therapeutics that overcome resistance in cancer and microbial infection. *Biomaterials* **2020**, *252*, 120078.

(3) Liu, H.; Shen, W.; Liu, W.; Yang, Z.; Yin, D.; Xiao, C. From oncolytic peptides to oncolytic polymers: A new paradigm for oncotherapy. *Bioact. Mater.* **2024**, *31*, 206−230.

(4) Takahashi, H.; Sovadinova, I.; Yasuhara, K.; Vemparala, S.; Caputo, G. A.; Kuroda, K. Biomimetic antimicrobial polymers − Design, characterization, antimicrobial, and novel applications. *WIREs Nanomedicine and Nanobiotechnology* **2023**, *15*, No. e1866.

(5) Le, W.; Chen, B.; Cui, Z.; Liu, Z.; Shi, D. Detection of cancer cells based on glycolytic-regulated surface electrical charges. *Biophys. Reports* **2019**, *5*, 10−18.

(6) Preta, G. New insights into targeting membrane lipids for cancer therapy. *Front. Cell Dev. Biol.* **2020**, *8*, 1−10.

(7) Takahashi, H.; Yumoto, K.; Yasuhara, K.; Nadres, E. T.; Kikuchi, Y.; Buttitta, L.; Taichman, R. S.; Kuroda, K. Anticancer polymers designed for killing dormant prostate cancer cells. *Sci. Rep.* **2019**, *9*, 1096.

(8) Palermo, E. F.; Vemparala, S.; Kuroda, K. Cationic spacer arm design strategy for control of antimicrobial activity and conformation of amphiphilic methacrylate random copolymers. *Biomacromolecules* **2012**, *13*, 1632−1641.

(9) Baul, U.; Kuroda, K.; Vemparala, S. Interaction of multiple biomimetic antimicrobial polymers with model bacterial membranes. *J. Chem. Phys.* **2014**, *141*, 084902.

(10) Baul, U.; Vemparala, S. Influence of lipid composition of model membranes on methacrylate antimicrobial polymer−membrane interactions. *Soft Matter* **2017**, *13*, 7665−7676.

(11) Rani, G.; Kuroda, K.; Vemparala, S. Towards designing globular antimicrobial peptide mimics: role of polar functional groups in biomimetic ternary antimicrobial polymers. *Soft Matter* **2021**, *17*, 2090−2103.

(12) Sikdar, S.; Rani, G.; Vemparala, S. Role of lipid packing defects in determining membrane interactions of antimicrobial polymers. *Langmuir* **2023**, *39*, 4406−4412.

(13) Saiba, R.; Debnath, A.; Vemparala, S. The role of negatively charged groups in antimicrobial cationic peptide mimics: insights into membrane interactions. *J. Phys. Chem. B* **2025**, *129*, 7134−7145.

(14) Pulica, R.; Aquib, A.; Varsanyi, C.; Gadiyar, V.; Wang, Z.; Frederick, T.; Calianese, D. C.; Patel, B.; de Dios, K. V.; Poalasin, V.; De Lorenzo, M. S.; Kotenko, S. V.; Wu, Y.; Yang, A.; Choudhary, A.; Sriram, G.; Birge, R. B. Dys-regulated phosphatidylserine externalization as a cell intrinsic immune escape mechanism in cancer. *Cell Commun. Signal.* **2025**, *23*, 131.

(15) Vanommeslaeghe, K.; MacKerell, A. D., Jr. Automation of the CHARMM General Force Field (CGenFF) I: Bond perception and atom typing. *J. Chem. Inf. Model.* **2012**, *52*, 3144−3154.

(16) Klauda, J. B.; Venable, R. M.; Freites, J. A.; O'Connor, J. W.; Tobias, D. J.; Mondragon-Ramirez, C.; Vorobyov, I.; MacKerell, A. D.; Pastor, R. W. Update of the CHARMM all-atom additive force field for lipids: validation on six lipid types. *J. Phys. Chem. B* **2010**, *114*, 7830−7843.

(17) MacKerell, A. D.; Bashford, D.; Bellott, M.; Dunbrack, R. L.; Evanseck, J. D.; Field, M. J.; Fischer, S.; Gao, J.; Guo, H.; Ha, S.; Joseph-McCarthy, D.; Kuchnir, L.; Kuczera, K.; Lau, F. T. K.; Mattos, C.; Michnick, S.; Ngo, T.; Nguyen, D. T.; Prodhom, B.; Reiher, W. E.; Roux, B.; Schlenkrich, M.; Smith, J. C.; Stote, R.; Straub, J.; Watanabe, M.; Wiórkiewicz-Kuczera, J.; Yin, D.; Karplus, M. All-atom empirical potential for molecular modeling and dynamics studies of proteins. *J. Phys. Chem. B* **1998**, *102*, 3586−3616.

(18) Bussi, G.; Donadio, D.; Parrinello, M. Canonical sampling through velocity rescaling. *J. Chem. Phys.* **2007**, *126*, 014101.

(19) Bernetti, M.; Bussi, G. Pressure control using stochastic cell rescaling. *J. Chem. Phys.* **2020**, *153*, 114107.

(20) Essman, U.; Perera, L.; Berkowitz, M. L.; Darden, T.; Lee, H.; Pedersen, L. G. A smooth particle mesh Ewald method. *J. Chem. Phys.* **1995**, *103*, 8577−8592.

(21) Páll, S.; Zhmurov, A.; Bauer, P.; Abraham, M.; Lundborg, M.; Gray, A.; Hess, B.; Lindahl, E. Heterogeneous parallelization and acceleration of molecular dynamics simulations in GROMACS. *J. Chem. Phys.* **2020**, *153*, 134110.

(22) CGenFF. 2026, SilcsBio, LLC. https://cgenff.com (accessed 26.05.2026).

(23) Wu, E. L.; Cheng, X.; Jo, S.; Rui, H.; Song, K. C.; Davila-Contreras, E. M.; Qi, Y. F.; Lee, J. M.; Monje-Galvan, V.; Venable, R. M.; Klauda, J. B.; Im, W. CHARMM-GUI Membrane Builder toward realistic biological membrane simulations. *J. Comput. Chem.* **2014**, *35*, 1997−2004.

(24) Kostritskii, A. Yu.; Kondinskaia, D. A.; Nesterenko, A. M.; Gurtovenko, A. A. Adsorption of synthetic cationic polymers on model phospholipid membranes: insight from atomic-scale molecular dynamics simulations. *Langmuir* **2016**, *32*, 10402−10414.

(25) Gurtovenko, A. A.; Nazarychev, V. M. Antimicrobial biomimetic polymers in action: a putative mechanism of acyl-lysine binding to bacterial membranes and aggregation effects. *Langmuir* **2025**, *41*, 23715−23725.

(26) Ulmschneider, M.; Ulmschneider, J.; Schiller, N.; Wallace, B. A.; von Heijne, G.; White, S. H. Spontaneous transmembrane helix insertion thermodynamically mimics translocon-guided insertion. *Nat. Commun.* **2014**, *5*, 4863.

(27) Wang, Y.; Chen, C.; Hu, D.; Ulmschneider, M. B.; Ulmschneider, J. P. Spontaneous formation of structurally diverse membrane channel architectures from a single antimicrobial peptide. *Nat. Commun.* **2016**, *7*, 13535.

(28) Chen, C. H.; Starr, C. G.; Troendle, E.; Wiedman, G.; Wimley, W. C.; Ulmschneider, J. P.; Ulmschneider, M. B. Simulation-guided rational de novo design of a small pore-forming antimicrobial peptide. *J. Am. Chem. Soc.* **2019**, *141*, 4839−4848.

(29) Humphrey, W.; Dalke, A.; Schulten, K. VMD - Visual Molecular Dynamics. *J. Mol. Graphics* **1996**, *14*, 33−38.

(30) Gurtovenko, A. A.; Anwar, J.; Vattulainen, I. Defect-mediated trafficking across cell membranes: insights from *in silico* modeling. *Chem. Rev.* **2010**, *110*, 6077−6103.

(31) Gurtovenko, A. A.; Lyulina, A. S. Electroporation of asymmetric phospholipid membranes. *J. Phys. Chem. B* **2014**, *118*, 9909−9918.

(32) Zhang, D. T.; Baldauf, L.; Lazarski, G.; van Erp, T. S.; Shinoda, W. Membrane pore formation unveiled by ∞RETIS path sampling: from thinning to flip-flop. *J. Chem. Theory Comput.* **2026**, *22*, 3072−3083.

(33) Tieleman, D. P.; Marrink, S.-J. Lipids out of equilibrium: energetics of desorption and pore mediated flip-flop. *J. Am. Chem. Soc.* **2006**, *128*, 12462−12467.

(34) Ebbensgaard, A.; Mordhorst, H.; Overgaard, M. T.; Nielsen, C. G.; Aarestrup, F. M.; Hansen, E. B. Comparative evaluation of the antimicrobial activity of different antimicrobial peptides against a range of pathogenic bacteria. *PLoS One* **2015**, *10*, No. e0144611.

(35) Xia, L.; Zhang, F.; Liu, Z.; Ma, J.; Yang, J. Expression and characterization of cecropinXJ, a bioactive antimicrobial peptide from Bombyx mori (Bombycidae, Lepidoptera) in Escherichia coli. *Exp. Ther. Med.* **2013**, *5*, 1745−1751.

(36) Franzin, C. M.; Macdonald, P. M. Polylysine-induced ^{2}H NMR-observable domains in phosphatidylserine/phosphatidylcholine lipid bilayers. *Biophys. J.* **2001**, *81*, 3346−3362.

(37) Schwieger, C.; Blume, A. Interaction of poly(L-lysines) with negatively charged membranes: An FT-IR and DSC study. *Eur. Biophys. J.* **2007**, *36*, 437−450.

Downloaded from pubs.acs.org/jpcbfk/article-pdf/130/38/9816/6849260/acs.jpcb.6c03563.pdf?guestAccessKey=68260e30-8a50-43a7-b021-503799ebd130 by Andrey Gurtovenko on 24 September 2026

https://doi.org/10.1021/acs.jpcb.6c03563
J. Phys. Chem. B 2026, 130, 9816−9825